Autoionization of foil-excited states in Li I and Li II

R. Bruch, G. Paul, and J. Andrä
Freie Universität Berlin, Institut für Atom- und Festkörperphysik A, 1 Berlin 33, Boltzmannstrasse 20, West Germany

Lester Lipsky
University of Nebraska, Department of Computer Science, Lincoln, Nebraska, 68508
(Received 10 December 1973; revised manuscript received 23 June 1975)

We have used the beam-foil interaction mechanism to populate highly excited states in lithium by passing 300-keV Li^+ ions through 8-$\mu g/cm^2$-thick carbon foils. The energies of the electrons emitted via autoionization were analyzed. By moving the foil along the beam axis, prompt and delayed electrons due to decays of Li I and Li II states were identified. These spectra are interpreted with the help of detailed theoretical calculations. The excitation energies of the Li I $(1s2s^2)^2S^e$ and Li II $(2s2p)^{1,3}P^o$ terms were determined to 0.5% accuracy. We have observed decays of doubly excited Li II states above the $n=2$ threshold. On the basis of our theoretical estimates, we assign a peak in the high-energy portion of the spectra as due to deexcitation of triply excited Li I $2s^22p$ and $2s2p^2$ configurations.

I. INTRODUCTION

The study of doubly excited autoionization states of low-Z atoms, particularly He, has yielded considerable information on two-electron correlations.[1] Despite the fundamental importance of these resonances in two-electron atoms, with the exception of H^- and He, no systematic experimental investigation of autoionizing transitions in the isoelectronic He series has been reported in the literature. We present here measurements and interpretations of energies of electrons emitted in the decay of some doubly and triply excited states in Li I and Li II.

Observation of the decay of two- and three-electron states in ions requires an efficient means for their excitation. Sellin and co-workers[2] have shown that beam-foil excitation is a powerful method for producing highly charged ions in highly excited states. Among the methods commonly used to excite autoionizing states (elastic and inelastic electron scattering,[3,4] uv absorption,[5] electron or proton impact,[6] and heavy-ion bombardment of gases[7] and vapors[8]) beam-foil excitation[9,10] resembles heavy-ion excitation most closely. There are certain advantages in heavy-ion excitations, such as (a) observation of electrons emitted from the projectile as well as the target, and (b) multiple excitation of electrons. In addition, beam-foil excitation also allows the production of highly excited ionic states over a wide energy range with the mean ionic charge controllable to some degree. Futhermore, both the prompt electron spectra and the delayed spectra from long-lived metastable states can be observed in the same experiment by moving the foil in and out of the focus of a spectrometer along the beam axis.

II. METHOD AND RESULTS

When a fast Li^+ ion beam with a velocity of about 2.8×10^8 cm/sec (300 keV) passes through a 8-$\mu g/cm^2$-thick carbon foil, a high fraction of Li and Li^+ projectiles in doubly and triply excited states emerges from the back surface of the foil. These multiply excited Li I **, Li I ***, and Li II ** states, having excitation energies in excess of the first ionization limit, then decay via Coulomb autoionization provided the parity, spin, and orbital angular momenta of the initial and final states are unchanged.[11] Such highly excited lithium states (decaying by Coulomb autoionization with mean lives of typically 10^{-14} sec) have decay lengths $L=v\tau$ of the order of 280 Å at 300 keV beam energy. Thus in a foil-excitation experiment (foil thickness $d\simeq300$ Å) there is a certain probability for the unperturbed observation of such short-lived ions in flight after the particles leave the foil. Therefore, we have chosen an experimental setup (Fig. 1) which allows the foil to be moved in the focus of our cylindrical electrostatic electron spectrometer, which is similar in design to the one used by Sellin and co-workers.[2] The foil can be moved up to 8 cm downstream (tunable time delay: 0–30 nsec) out of the focus of our cylindrical analyzer. In this manner we are able to separate the less probable delayed electron decays caused by spin-orbit (H_{so}), spin-other-orbit (H_{soo}), spin-spin (H_{ss}), and hyperfine coupling (H_{hf}) from the prompt decays.

The electron spectrometer views the beam at an angle of $\Theta=42.3°$ and is provided with two pairs of continuously variable entrance and exit slits in order to reduce the viewing region of the beam to a length (l) of about 1.8 mm at 1-mm beam diam-

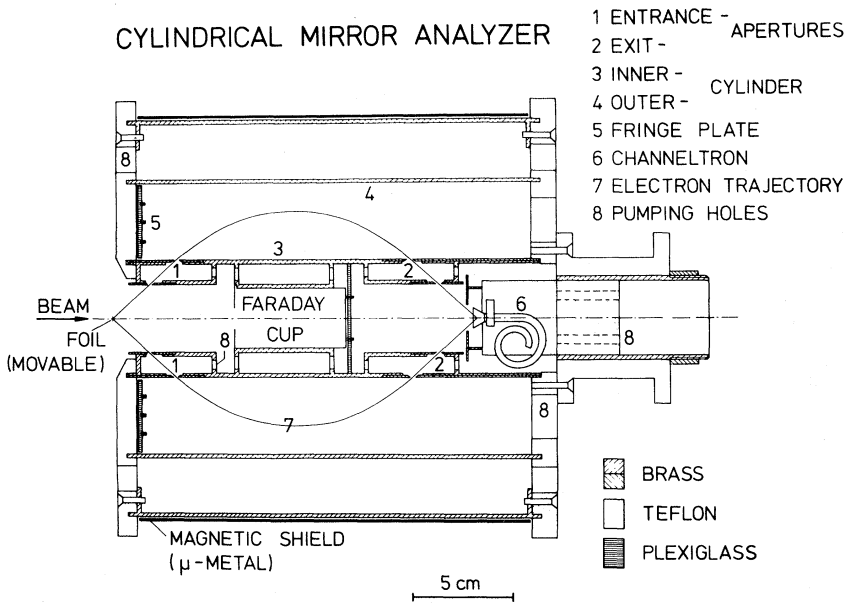

FIG. 1. Electrostatic analyzer used for measurements of energy distributions of electrons ejected after beam-foil excitation.

eter, corresponding to an angular spread $2\Delta\Theta = 2°$ and a transmission $T = 1\%$. This finite extension of the beam length viewed by the spectrometer causes a time uncertainty of the observation $t = l/v = 0.6$ nsec.

For calibration of the analyzer a monochromatic point-electron source[12] was used. Above 50 eV we achieved a 0.3% full width at half-maximum (FWHM) resolution and an absolute energy calibration ±0.1% with slit widths of 0.5 mm. To avoid any influence of Earth's magnetic field on the resolution and calibration of the spectrometer, both the target chamber and the analyzer were shielded with μ metal.

However, the kinematic transformation[7,13] from the rest frame of the emitting ion ($E_{\text{c.m.}}$) to the laboratory frame (E_{lab}) causes a considerable line spread arising from (i) the energy straggling of the projectiles in the target, (ii) the angle scattering of the ion beam by the foil, and (iii) the finite angular divergence ($\Delta\Theta = 1°$) defined by the acceptance of the spectrometer. We thus obtain an effective energy resolution by convoluting these dynamical contributions with the spectrometer window function. For Li^+ ions (300 keV) passing through 8-$\mu g/cm^2$ carbon foils, we measured an effective resolution of about 1.7% FWHM.

With this experimental arrangement, prompt and delayed electron spectra of incident 300–310-keV $^7Li^+$ ions on carbon foils were recorded at beam currents of a few nAmp. Typical results of the lithium electron spectra are shown in Figs. 2 and 3. The Li spectrum is presented here because it is the simplest system we studied, and even at this stage it permits a rather complete interpretation. In Fig. 2 we have displayed the energy distribution (lab system) of the prompt electron ejection after $^7Li^+ \rightarrow$ C-foil collisions. This spectrum exhibits two distinct autoionization line structures superimposed on a continuous electron background. Because of the fast motion of the Li projectiles during deexcitation, the autoionization lines are doppler shifted by about 50 eV. This allows discrimination against the slowly varying low-energy background. This paper will be concerned with the high-energy portion of the prompt and delayed electron spectra which are shown in Figs. 3(a) and 3(b), respectively. The intensities of the data, (a) the prompt and (b) the delayed spec-

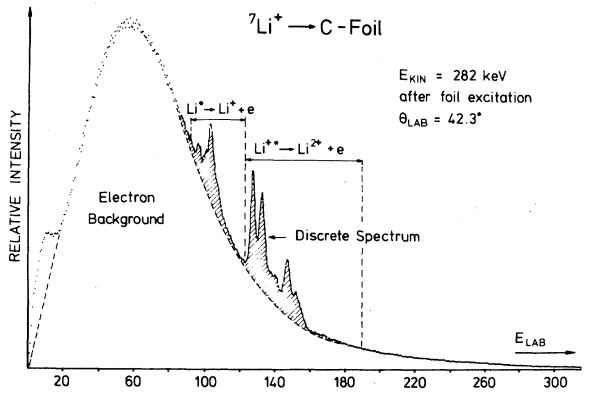

FIG. 2. Prompt electron energy spectrum from lithium produced by foil excitation. Discrete peaks are due to Coulomb autoionization of highly excited Li I and Li II states. Energies are in eV.

tra, differ by a factor of about one hundred and are therefore not directly comparable.

III. METASTABLE AUTOIONIZING QUARTET LEVELS

Study of autoionization of Li I $(1s2lnl')\,^4L$ states to the $(1s^2\epsilon l)\,^2l$ continuum ($\Delta S=1$) via spin-orbit, spin-other-orbit, and spin-spin mixing reveals information on the strength of relativistic interactions in high-lying quartet levels. Such metastable "weak" autoionizing states are of interest for several reasons. The most important reasons are the following: (i) Autoionization rates due to relativistic mixings are of the order 10^4–10^9 sec^{-1}. Hence electric dipole transitions can compete as deexcitation mechanisms.[14,15] (ii) Because of the narrow inherent widths, metastable autoionizing levels allow precision measurements of the fine- and even hyperfine-structure splitting.[16] (iii) The different strength of configuration interaction within a given fine-structure multiplet (differential metastability[16]) provides a mechanism to produce polarized electrons[17] and nuclei.[16]

In Fig. 4 we have shown a level diagram of the most prominent odd- and even-parity quartet states in Li I converging to the $(1s2s)\,^3S$ and $(1s2p)\,^3P$ series limits. The excitation energies indicated in the level scheme are based on theoretical estimates[18] and on optical line identifications.[9,10,14] From the $(1s2snl)\,^4l$ and $(1s2pnl)\,^4l$, $^4(l\pm1)$ levels, those lying below the $(1s2s)\,^3S$ ionization threshold can undergo nonradiative transitions only to the $(1s^2\epsilon l)\,^2l$ continuum, whereas $(1s2pnl)$ configurations with $n\geq3$ are coupled alternatively to the $(1s^2\epsilon l)\,^2l$ and the $(1s2s^3S\epsilon l)\,^{2,4}l$ continua. According to Garcia and Mack[19] the members of the series $(1s2p^3Pnl)\,^4l$ with $n\geq3$ and $l\geq1$ are metastable with respect to Coulomb autoionization (see Fig. 4). The odd-parity configurations $(1s2snp)$, $(1s2pns)$, and $(1s2pnd)$ as well as the even parity configurations $(1s2sns)$ and $(1s2pnp)$ are strongly mixed. The perturbation of the quartet states lose significance for the higher n values, because of the nondegeneracy of the thresholds $(1s2s)\,^3S$ and $(1s2p)\,^3P$, respectively. Holøien and Geltman[18] have suggested classification of the lowest $^4P^o$ states in the following way: $(1s, 2s2p+)\,^4P^o(1)$, $(1s, 23sp+)\,^4P^o(2)$, $(1s, 23sp-)\times{}^4P^o(3)$, etc., where the (±) classification has been introduced.

The experimental electron spectrum ($t=3.7$ nsec) due to decays of some metastable Li I quartet states to the doublet continuum is displayed in Fig. 5. The quartet energies as indicated in this plot have been calculated by Holøien and Geltman.[18] We have assigned the first strong peak in the spectrum at about 51.1 eV due to metastable autoionization of the $(1s2s2p)\,^4P^o=\,^4P^o(1)$ level. The excitation energy of the Li I $^4P^o(1)$ state has been measured by threshold electron excitation[20] (57.3 ±0.3 eV). A crucial point in our experiments is the velocity determination of the beam after the foil. In order to avoid this difficulty, the value[4] 57.442 ± 0.004 eV for $^4P^o(1)$ has been adopted as an energy calibration point for all the Li spectra,

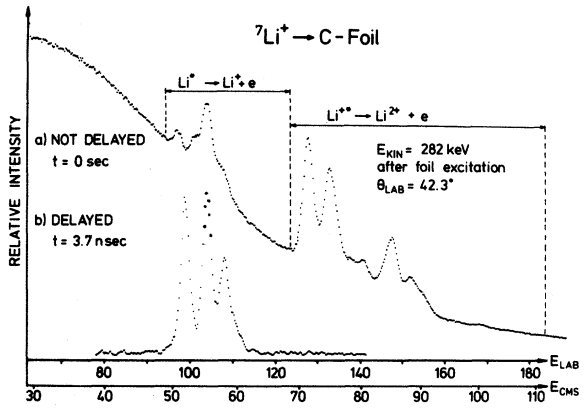

FIG. 3. Prompt and delayed Li I and Li II electron emission spectrum plotted both in the lab frame (E_{lab}) and in the rest frame of the emitting projectiles ($E_{c.m.}$). Energies are in eV.

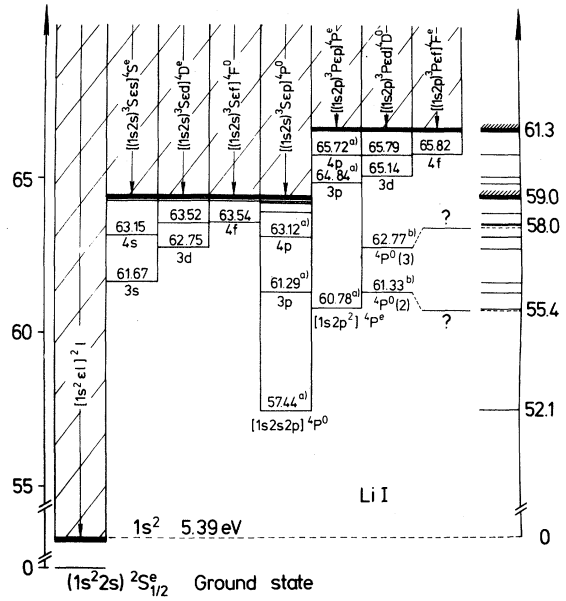

FIG. 4. Energy-level diagram for metastable autoionizing ^4L states in Li I. Experimental values (a) are deduced from dipole transitions (Refs. 9 and 10). Theoretical values (b) are taken from Holøien and Geltman (Ref. 18). The remainder have been estimated using the quantum-defect method (Ref. 7). The energy scale on the right-hand side of the figure represents possible transition energies of Li I quartet states decaying to the adjacent $(1s^2\epsilon1)\,^21$ continuum. Energies are in eV.

since the prompt and the delayed spectra could be obtained successively with the same foil. Thus it is possible, in principle, to determine the transition energies of the most prominent features in the prompt and delayed Li electron spectra to an accuracy of ±0.1 eV.

The second strong line in the spectrum at about 55.4 eV could be composed of four lines due to autoionization of the states $^4P^e$ (1), $^4P^o$ (2), $^4S^e$ (1), and $(1s2p^2)\,^2P^e$, respectively. However, the $(1s2p^2)\,^2P^e$ level decays by photon emission to the low-lying $(1s^2 2p)\,^2P^o$ level in about 0.015 nsec.[21] Therefore, the peak at 55.4 eV is essentially an admixture of at least two transitions associated with autoionization of the $^4P^e$ (1) and $^4P^o$ (2) levels which should nearly coincide in energy. This is justified by the agreement of the energy separation of the two strongest peaks in this experiment (3.33 eV) as compared to the optical $^4P^e$ (1)-$^4P^o$ (1) transition energy of 3.34 eV.[15]

The third peak at about 1 eV below the $(1s2s)\,^3S$ series limit is surprisingly sharp, although several transitions (see Fig. 5) should overlap in this energy region. Above $(1s2s)\,^3S$, two unresolved peaks appear which might originate from metastable Li I levels of the kind $(1s2pnl)\,^4l$ decaying to the $(1s^2\epsilon l)\,^2l$ continuum.

Recent beam-foil studies of Li^+ ions using grazing incidence spectrometers[9,10] have revealed dipole transitions arising from Li II levels which are metastable with respect to Coulomb autoionization. However, no delayed electrons owing to decays of doubly excited Li II states have been recognized in our spectra. We thus conclude that these levels decay mainly by radiation and not by electron emission.

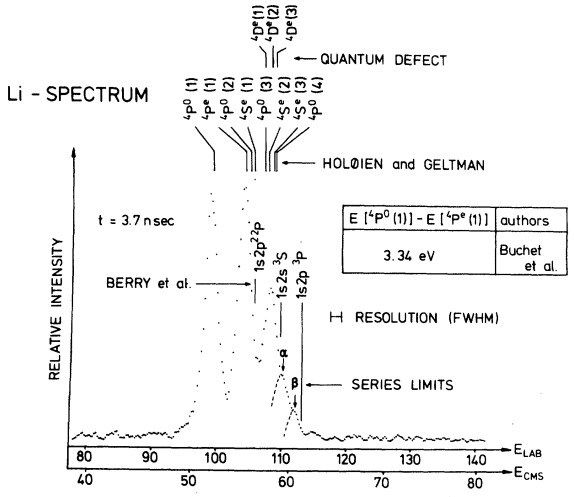

FIG. 5. Electron energy spectrum for decay of autoionizing quartet states in Li I. The notation of Holøien and Geltman (Ref. 18) has been adopted. Energies are in eV.

IV. PROMPT AUTOIONIZING DOUBLET LEVELS

The energy-level diagram as displayed in Fig. 6 is devoted to Coulomb autoionization of odd- and even-parity Li I states of the kind $1s2lnl'$ with $n>2$. The Li I resonances of the type $(1s2lnl')\,^2L$ converge to four distinct series limits $(1s2s)\,^{1,3}S$ and $(1s2p)\,^{1,3}P$, respectively. There is a strong mixing in the $(1s2s)\,^1Snl$ and $(1s2p)\,^3Pnl$ configurations owing to the narrow spacing of the $(1s2s)\,^1S$ and $(1s2p)\,^3P$ thresholds (Fig. 6). The odd-parity Li I $^2P^o$ resonances are known from uv absorption[5] to better than 0.1 eV accuracy, whereas the even-parity states such as $(1s2s^2)\,^2S^e$, $(1s2p^2)\,^2S^e$, and $^2D^e$, etc., cannot be excited optically from the Li I ground state $(1s^2 2s)\,^2S^e$. In order to classify resonant structures above the $(1s2s)\,^3S$ threshold, Cooper *et al.*[22] have performed close-coupling calculations. Some of their results are plotted in Fig. 6. For Li I $1s2lnl'$ states above the onset of the $(1s2s)\,^3S$ series limit at least two continua are adjacent, namely, $(1s^2\epsilon l)\,^2l$ and $(1s2s\,^3S\epsilon l)\,^2l$. Owing to the fact that autoionization is strongest near threshold,[23] we would expect that transitions to the $(1s2s\,^3S\epsilon l)\,^2l$ continuum to be favored.

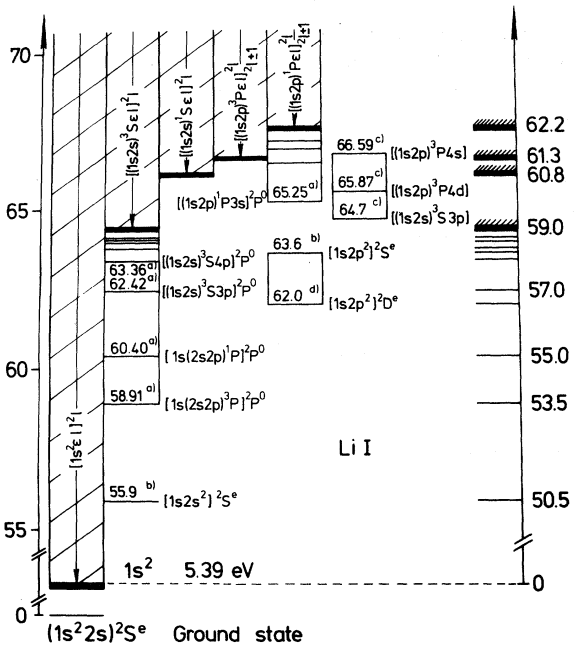

FIG. 6. Energy-level diagram for Coulomb autoionizing ^2L states in Li I as derived from (a) uv-absorption measurements (Ref. 4), (b) present work, (c) close-coupling calculations (Ref. 22), and (d) variational minimum principle (Ref. 39). The energy ladder on the right predicts peak positions of possible decays of ^2L states to the $(1s^2\epsilon l)^2l$ continuum.

The low-energy group of lines in the prompt spectrum (Fig. 7) can be assigned to Li I doublet configurations. An analysis of this part of the spectrum has been attempted. The main group of lines which occur at about 55 eV coincide with three $^2P^o$ states from uv-absorption experiments[5] to within 0.2 eV. It is apparent from the level diagram that the first peak in the spectrum at 50.5 ± 0.5 eV cannot be associated to Coulomb autoionization of odd-parity levels. Therefore, we have interpreted this line as the transition $(1s2s^2)\,^2S^e \rightarrow (1s^2\epsilon s)\,^2S^e$ giving an excitation energy of 55.9 ± 0.5 eV for the $(1s2s^2)\,^2S^e$ level. This interpretation is consistent with Fricke's Hartree-Fock calculation[24] which predicts the $(1s2s^2)\,^2S^e$ excitation energy 0.6 eV above our experimental value. The higher-lying even-parity states of the kind $(1s2p^2)\times{}^2S^e$ and $^2D^e$ could not be verified experimentally.

Possible charging up of the foil during heavy-ion bombardment would tend to slow down the prompt electrons, but not the delayed ones. This effect contributes an unknown uncertainty in the calibration of the prompt spectra. Comparison of our Li $^2P^o$ energies with those obtained by uv absorption, however, shows no discernible shift in the prompt spectra.

V. THEORETICAL CALCULATIONS

Extensive experimental investigations[7,11] and theoretical calculations[7,11,25] have been performed to identify the resonant states in helium due to double-electron excitation. Since two-electron atoms are the simplest systems that can autoionize, our interest has been to extend these studies to higher members of the He isoelectronic series. In particular, this allows the study of two-electron correlations in highly excited states as a function of the atomic number. Our experimental data are explained here in terms of complete calculations of doubly excited states in Li II and triply excited states in Li I.

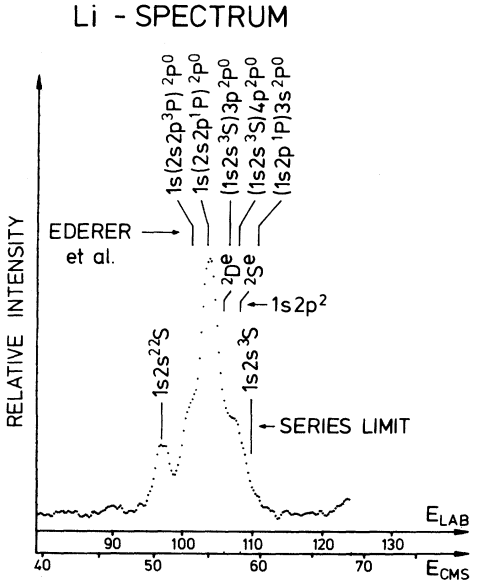

FIG. 7. Li I autoionization spectrum between 40 and 60 eV (background subtracted).

The doubly excited states for Li^+ have been calculated using the truncated diagonalization method (TDM) of Lipsky and Russek,[25] or Altick and Moore.[26] For resonances below the $n=2$ threshold, all possible hydrogenic product functions have been included in which one of the electrons is represented by a $2s$, $2p$, $3s$, $3p$, or $3d$ function, and the other electron can have any radial quantum number from 2 to 10. No $1s$ configurations were used, although other states through $5g5g$ were. In order to calculate resonances below the $N=3$ threshold, all configurations with N or n equal 2 were eliminated, and the reduced matrix diagonalized. The full details are given by Lipsky, Conneely, and Anania.[27]

The triply excited states were calculated using an extension of the TDM as described by Ahmed and Lipsky.[28] Here, only configurations up through $n=5$ were included, while (as in doubly excited states) all $(1s)$ states were excluded. Furthermore, the wave functions are expanded in terms of doubly excited states, so the resultant energy levels are upper bounds to the true levels.

All the calculated doubly and triply excited levels come from *ab initio* calculations, and therefore do not depend on any experimental constants when expressed in atomic units below total ionization (1 a.u. = 27.21 eV). In converting to electron volts, we used

$$E\ (\text{eV above } 1s) = 2\times 13.605\times\left(\tfrac{9}{2} - |E(\text{a.u.})|\right). \tag{1}$$

The doubly excited states for Li^+ (as with all other two-electron systems with nuclear charge $Z \geq 2$) can be classified into different Rydberg series which converge to the $N=2$ and 3 levels of Li^{++}. When the energy levels are expressed as effective quantum numbers (n^*), i.e.,

$$E\ (\text{a.u.}) = -(3)^2/2N^2 - (2)^2/2(n^*)^2, \tag{2}$$

then, in most cases, the identities of the different series become apparent, since the fractional parts of the n^*'s should differ only slightly from one member of a series to another member of the same series. The series classifications are based partly on this relationship and partly on a detailed examination of the wave functions, which was carried out to compare the configuration mixings of the

TABLE I. Doubly excited states below the $N=2$ threshold in Li^+. See Eq. (3) of the text for explanation of the classifications. An (*) marks each state which is the lowest member of its series. Energy in a.u. is total energy below double ionization. The column marked eV lists the energy above the 1s threshold of Li^{++}.

Classification	Effective quantum number	Energy (a.u.)	Energy (eV)	Classification	Effective quantum number	Energy (a.u.)	Energy (eV)
(2, 2*a*)100*	1.604 259	1.902 106	70.6887	(2, 4*c*)111	4.182 206	1.239 345	88.7224
(2, 2*a*)311*	1.633 379	1.874 644	71.4359	(2, 4*b*)100	4.224 985	1.237 041	88.7851
(2, 2*a*)310*	1.733 333	1.790 680	73.7206	(2, 5*a*)300	4.531 818	1.222 383	89.1889
(2, 2*a*)120*	1.773 660	1.760 753	74.5349	(2, 5*b*)111	4.582 310	1.220 248	89.2420
(2, 2*a*)111*	1.792 699	1.747 321	74.9004	(2, 5*a*)100	4.639 533	1.217 914	89.3055
(2, 2*b*)100*	2.022 883	1.613 751	78.5348	(2, 5*a*)311	4.683 824	1.216 165	89.3531
(2, 3*a*)300*	2.522 386	1.439 344	83.2804	(2, 5*a*)320	4.714 098	1.214 997	89.3849
(2, 3*b*)111*	2.562 720	1.429 527	83.5475	(2, 5*a*)110	4.743 378	1.213 890	89.4150
(2, 3*a*)100	2.641 231	1.411 693	84.0328	(2, 5*b*)311	4.762 351	1.213 183	89.4342
(2, 3*a*)320*	2.677 374	1.404 004	84.2420	(2, 5*a*)331	4.843 406	1.210 257	89.5139
(2, 3*a*)311	2.682 455	1.402 948	84.2707	(2, 5*a*)120	4.873 517	1.209 206	89.5425
(2, 3*a*)110*	2.695 314	1.400 303	84.3427	(2, 5*a*)121	4.874 990	1.209 155	89.5438
(2, 3*b*)311*	2.710 716	1.397 183	84.4276	(2, 5*a*)310	4.878 016	1.209 050	89.5467
(2, 3*a*)331*	2.835 735	1.373 713	85.0662	(2, 5*b*)320	4.919 013	1.207 656	89.5847
(2, 3*a*)121*	2.853 693	1.370 592	85.1511	(2, 5*a*)321	4.960 595	1.206 276	89.6222
(2, 3*a*)310	2.856 890	1.370 043	85.1661	(2, 5*a*)111	4.962 954	1.206 199	89.6243
(2, 3*a*)120	2.867 171	1.368 289	85.2139	(2, 5*a*)130	4.965 235	1.206 123	89.6263
(2, 3*b*)320*	2.906 634	1.361 728	85.3923	(2, 5*a*)330	4.966 748	1.206 075	89.6277
(2, 3*b*)300*	2.925 479	1.358 687	85.4751	(2, 5*b*)300	4.974 803	1.205 812	89.6348
(2, 3*a*)111	2.939 003	1.356 542	85.5335	(2, 5*b*)331	4.994 279	1.205 183	89.6519
(2, 3*a*)321*	2.945 590	1.355 507	85.5616	(2, 5*b*)131	4.996 069	1.205 126	89.6535
(2, 3*a*)131*	3.020 945	1.344 151	85.8706	(2, 5*b*)120	5.032 199	1.203 979	89.6847
(2, 3*b*)120*	3.021 059	1.344 134	85.8711	(2, 5*a*)131	5.036 745	1.203 836	89.6886
(2, 3*c*)311*	3.088 426	1.334 679	86.1283	(2, 5*c*)331*	5.039 818	1.203 740	89.6912
(2, 3*c*)111*	3.178 053	1.323 019	86.4456	(2, 5*c*)131*	5.040 104	1.203 732	89.6914
(2, 3*b*)100	3.206 373	1.319 536	86.5404	(2, 5*c*)320	5.070 369	1.202 794	89.7169
(2, 4*a*)300	3.527 069	1.285 769	87.4592	(2, 5*c*)120	5.076 944	1.202 593	89.7224
(2, 4*b*)111	3.574 533	1.281 528	87.5746	(2, 5*c*)311	5.081 129	1.202 465	89.7259
(2, 4*a*)100	3.637 290	1.276 173	87.7203	(2, 5*c*)111	5.183 908	1.199 424	89.8086
(2, 4*a*)311	3.680 926	1.272 610	87.8172	(2, 5*b*)100	5.230 927	1.198 092	89.8449
(2, 4*a*)320	3.701 707	1.270 957	87.8622	(2, 6*a*)300	5.536 384	1.190 249	90.0583
(2, 4*a*)110	3.727 963	1.268 909	87.9180	(2, 6*b*)111	5.588 162	1.189 046	90.0910
(2, 4*b*)311	3.745 984	1.267 527	87.9555	(2, 6*a*)100	5.642 308	1.187 822	90.1243
(2, 4*a*)331	3.838 759	1.260 721	88.1407	(2, 6*a*)311	5.686 599	1.186 848	90.1508
(2, 4*a*)121	3.867 235	1.258 730	88.1949	(2, 6*a*)320	5.721 407	1.186 097	90.1712
(2, 4*a*)310	3.870 770	1.258 486	88.2016	(2, 6*a*)110	5.752 100	1.185 447	90.1889
(2, 4*a*)120	3.871 001	1.258 470	88.2020	(2, 6*b*)311	5.771 410	1.185 043	90.1999
(2, 4*b*)320	3.913 693	1.255 573	88.2808	(2, 6*a*)331	5.846 538	1.183 510	90.2416
(2, 4*a*)321	3.955 510	1.252 828	88.3555	(2, 6*a*)120	5.874 480	1.182 955	90.2568
(2, 4*a*)111	3.956 001	1.252 795	88.3564	(2, 6*a*)121	5.879 453	1.182 857	90.2594
(2, 4*b*)300	3.960 549	1.252 502	88.3644	(2, 6*a*)310	5.881 724	1.182 812	90.2606
(2, 4*a*)130*	3.963 221	1.252 331	88.3690	(2, 6*b*)320	5.922 110	1.182 026	90.2820
(2, 4*a*)330*	3.964 352	1.252 257	88.3710	(2, 6*a*)321	5.963 176	1.181 243	90.3033
(2, 4*b*)331*	3.992 804	1.250 450	88.4202	(2, 6*a*)111	5.965 801	1.181 194	90.3047
(2, 4*b*)131*	3.994 130	1.250 367	88.4225	(2, 6*a*)130	5.966 672	1.181 177	90.3051
(2, 4*b*)120	4.029 120	1.248 199	88.4815	(2, 6*a*)330	5.968 345	1.181 146	90.3060
(2, 4*a*)131	4.032 302	1.248 005	88.4867	(2, 6*b*)300	5.981 894	1.180 892	90.3129
(2, 4*c*)320*	4.070 227	1.245 724	88.5488	(2, 6*b*)331	5.995 311	1.180 642	90.3197
(2, 4*c*)120*	4.074 559	1.245 466	88.5558	(2, 6*b*)131	5.997 295	1.180 605	90.3207
(2, 4*c*)311	4.082 131	1.245 020	88.5680	(2, 6*b*)120	6.033 372	1.179 943	90.3387

TABLE I *(continued)*

Classification	Effective quantum number	Energy (a.u.)	Energy (eV)	Classification	Effective quantum number	Energy (a.u.)	Energy (eV)
(2, 6*a*)131	6.038 168	1.179 855	90.3411	(2, 7*a*)100	6.643 619	1.170 312	90.6007
(2, 6*c*)331	6.040 273	1.179 816	90.3421	(2, 7*a*)311	6.687 761	1.169 716	90.6170
(2, 6*c*)131	6.040 999	1.179 804	90.3425	(2, 7*a*)320	6.725 186	1.169 220	90.6305
(2, 6*c*)320	6.070 688	1.179 269	90.3571	(2, 7*a*)110	6.756 776	1.168 807	90.6417
(2, 6*c*)120	6.078 375	1.179 132	90.3608	(2, 7*b*)311	6.776 184	1.168 556	90.6485
(2, 6*c*)311	6.080 793	1.179 089	90.3619	(2, 7*a*)331	6.848 045	1.167 648	90.6733
(2, 6*c*)111	6.184 581	1.177 288	90.4109	(2, 7*a*)120	6.874 125	1.167 324	90.6820
(2, 6*b*)100	6.233 455	1.176 472	90.4332	(2, 7*a*)121	6.881 708	1.167 232	90.6846
(2, 7*a*)300	6.539 535	1.171 766	90.5612	(2, 7*a*)310	6.883 150	1.167 213	90.6851
(2, 7*b*)111	6.591 753	1.171 028	90.5813	(2, 7*b*)320	6.923 556	1.166 722	90.6984

different states.

In Table I, all doubly excited states which are less than 91 eV above the 1*s* threshold, and with total orbital angular momentum 0, 1, 2, and 3, are included. As mentioned before, the energies (in atomic units) below total ionization come directly from the TDM calculations so they are included in this table for comparison with other calculations. The effective quantum numbers, calculated from Eq. (2), and the energies in eV from Eq. (1) are also contained in the table.

Whenever there is more than one series for a given S, L, and π, the mixings between the different configurations are so great that traditional classifications based on single products of orbitals are useless.[29] Therefore, the letters a, b, c, etc., are used instead to label the different series. When $Z>1$, there exists a one-to-one correspondence between the radial quantum numbers (N and n) of the single-particle states and the true states, and these are used in our classification scheme. The letters a, b, etc., are assigned according to the energy of the lowest member of each series. We use the following notation:

$$(N, n\alpha)\ (2S+1), L, \pi, \tag{3}$$

where N is the inner-electron quantum number (also the level of Li^{++} below which this state lies), n is the outer-electron radial quantum number, and $\alpha = a, b, c, \ldots$ (member of αth series).

Table II contains a description of all the series represented in Table I. The column called "approximate mixings," except where otherwise noted, lists descriptions which account for at least 90% of each wave function in the series. Since few calculations have been made of Li^+, the column labeled "width" is to be taken only as a guide as to what one might expect after considering information about other atoms or other series. It seems clear, though, that widths are as characteristic of a series as are the configuration mixings, so we guess that the following rules are generally true: (i) Series for which configurations add (plus states) are broader than those for which configurations subtract[1] (minus states). (ii) Series with configurations of smaller orbital quantum numbers will be broader than those with larger orbital quantum numbers. (iii) Lower lettered series are usually broader than higher lettered ones. (iv) Series which have no adjacent open channels of like configuration mixings to couple to, will be very narrow. This rule is strictly true for the metastable states such as $(2p2p)\,^3P^e$ which cannot decay at all through electron-electron interactions, but must either photodecay, or decay via one of L, S, and parity-violating perturbations such as the spin-orbit interaction.

These rules are not independent, but may be interrelated in one way or another.

Tables III and IV display data similar to Tables I and II, but for doubly excited states above $N=2$, and below the $N=3$ threshold. Here, since most states can decay through more than one channel (the bound electron can drop to either the 1*s*, or the 2*s* or 2*p* states), estimates of the widths are even less reliable, so they have been omitted.

Table V displays the results of Ahmed and Lipsky[28] for triply excited states with $^2S^e$ and $^2P^o$ symmetries. No attempt has been made to describe the configuration mixings, and so it has not been possible as yet to classify the states into series (except for the lowest states of each symmetry).

Table VI summarizes the possible decay modes for the various doubly excited configurations.

VI. Li II STATES BELOW THE $N=2$ SERIES LIMIT

In Fig. 8 we have displayed the higher-energy portion of the prompt lithium spectrum between 60

TABLE II. Classification of different series for Li^+ below the $N=2$ state of Li^{++}.

Series classification	Lowest n	Approximate mixings	Probable widths	Comments
$^1S^e$, two series involving configurations: $2snp$, $2pnp$				
$(2,na)\,^1S^e$	2	$(2snp+2pnp)$	Broad	
$(2,nb)\,^1S^e$	2	$(2snp-2pnp)$	Narrow	$(2,2b)$ contains 1.6% $3d3d$
$^3S^e$, two series involving configurations: $2snp$, $2pnp$				
$(2,na)\,^3S^e$	3	$(2snp+2pnp)$	Narrow?	
$(2,nb)\,^3S^e$	3	$(2snp-2pnp)$	Very narrow?	
$^1P^o$, three series involving configurations: $2snp$, $nd2p$, $2pnd$				
$(2,na)\,^1P^o$	2	$(2snp+nd2p)$	Broad	All except $(2,2a)$, contain over 10% $2pnd$
$(2,nb)\,^1P^o$	3	$(2snp-nd2p)$	Narrow	Have about 10% $2pnd$
$(2,nc)\,^1P^o$	3	$2pnd$	Very narrow	Have 20% sp
$^3P^o$, three series involving configurations: $2snp$, $nd2p$, $2pnd$				
$(2,na)\,^3P^o$	2	$(2snp+nd2p)$	Broad	
$(2,nb)\,^3P^o$	3	$(2snp-nd2p)+2pnd$	Narrow	
$(2,nc)\,^3P^o$	3	$(2snp-nd2p)-2pnd$	Very narrow	
$^1P^e$, one series involving configuration: $2pnp$				
$(2,na)\,^1P^e$	3	$2pnp$	Metastable	
$^3P^e$, one series involving configuration: $2pnp$				
$(2pnp)\,^3P^e$	2	$2pnp$	Metastable	
$^1D^o$, one series involving configuration: $2pnd$				
$(2,na)\,^1D^o$	3	$2pnd$	Metastable	
$^3D^o$, one series involving configuration: $2pnd$				
$(2,na)\,^3D^o$	3	$2pnd$	Metastable	
$^1D^e$, three series involving configurations: $2pnp$, $2snd$, $2pnf$				
$(2,na)\,^1D^e$	2	$(2pnp-2snd$	Narrow?	The $(2,2a)$ state is mostly $2p\,2p$
$(2,nb)\,^1D^e$	3	$(2pnp+2snd)$	Broad?	
$(2,nc)\,^1D^e$	4	$2pnf$	Very narrow?	
$^3D^e$, three series involving configurations: $2pnp$, $2snd$, $2pnf$				
$(2,na)\,^3D^e$	3	$(2pnp-2snd)$	Narrow?	2:1 ratio pp to sd.
$(2,nb)\,^3D^e$	3	$(2pnp+2snd)$	Broad?	1:2 ratio pp to sd; up to 10% pf
$(2,nc)\,^3D^e$	4	$2pnf$	Very narrow?	10% other
$^1F^o$, three series involving configurations: $2snf$, $2pnd$, $2png$				
$(2,na)\,^1F^o$	3	$2pnd$		25% others
$(2,nb)\,^1F^o$	4	$2snf$		a and c are crossing above $n=6$
$(2,nc)\,^1F^o$	5	$2png$		
$^3F^o$, three series involving configurations: $2snf$, $2pnd$, $2png$				
$(2,na)\,^3F^o$	3	$2pnd$		15% other
$(2,nb)\,^3F^0$	4	$2snf$		15% other
$(2,nc)\,^3F^o$	5	$2png$		
$^1F^e$, one series involving configuration: $2pnf$				
$(2,na)\,^1F^e$	4	$2pnf$	Metastable	
$^3F^e$, one series involving configuration: $2pnf$				
$(2,na)\,^3F^e$	4	$2pnf$	Metastable	

TABLE III. Doubly excited states below the $N = 3$ threshold in Li^+. See Eq. (3) of the text for explanation of the classifications. An (*) marks each state which is the lowest member of its series. Energy in a.u. is total energy below double ionization. The column marked eV lists the energy above the 1s threshold of Li^{++}.

Classification	Effective quantum number	Energy (a.u.)	Energy (eV)
(3, 4*b*)330*	3.848 669	0.635 023	105.1660
(3, 4*a*)131	3.904 760	0.631 172	105.2708
(3, 4*d*)331*	3.951 238	0.628 104	105.3542
(3, 4*c*)121*	3.962 439	0.627 381	105.3739
(3, 4*c*)120	4.016 859	0.623 953	105.4672
(3, 4*b*)310	4.018 856	0.623 830	105.4705
(3, 4*c*)321*	4.069 728	0.620 753	105.5543
(3, 4*e*)320*	4.078 543	0.620 232	105.5684
(3, 4*c*)300*	4.126 824	0.617 435	105.6445
(3, 4*d*)131*	4.143 932	0.616 467	105.6709
(3, 4*b*)111	4.164 094	0.615 342	105.7015
(3, 4*e*)120*	4.197 557	0.613 511	105.7513
(3, 5*a*)300	4.237 407	0.611 386	105.8092
(3, 5*c*)111	4.261 830	0.610 113	105.8438
(3, 4*e*)311*	4.300 321	0.608 150	105.8972
(3, 5*b*)320	4.316 852	0.607 324	105.9197
(3, 5*a*)100	4.323 992	0.606 970	105.9293
(3, 5*a*)311	4.348 654	0.605 760	105.9622
(3, 4*e*)111*	4.384 070	0.604 058	105.0085
(3, 5*a*)110	4.398 467	0.603 378	106.0270
(3, 5*c*)311	4.402 746	0.603 177	106.0325
(3, 5*b*)131	4.418 806	0.602 428	106.0529
(3, 5*a*)120	4.422 271	0.602 268	106.0572
(3, 5*b*)321	4.471 510	0.600 028	106.1182
(3, 4*c*)100	4.483 692	0.599 485	106.1330
(3, 5*d*)120	4.485 655	0.599 398	106.1353
(3, 5*a*)310	4.521 118	0.597 845	106.1776
(3, 5*a*)331	4.528 520	0.597 525	106.1863
(3, 5*a*)111	4.550 003	0.596 606	106.2113
(3, 5*a*)121	4.578 688	0.595 400	106.2441
(3, 5*b*)300	4.587 292	0.595 042	106.2539
(3, 5*c*)320	4.587 827	0.595 020	106.2545
(3, 5*b*)121	4.594 721	0.594 735	106.2622
(3, 5*a*)130	4.615 439	0.593 887	106.2853
(3, 5*a*)320	4.622 393	0.593 604	106.2930
(3, 5*d*)111	4.644 111	0.592 731	106.3168
(3, 5*b*)331	4.651 984	0.592 417	106.3253
(3, 5*a*)330	4.701 480	0.590 482	106.3779
(3, 5*c*)331	4.748 149	0.588 712	106.4261
(3, 5*b*)130	4.752 835	0.588 537	106.4309
(3, 5*a*)321	4.754 378	0.588 479	106.4324
(3, 5*c*)131	4.759 041	0.588 306	106.4371
(3, 5*b*)120	4.769 366	0.587 924	106.4475
(3, 5*d*)320	4.793 380	0.587 045	106.4714
(3, 5*b*)100	4.807 164	0.586 547	106.4850
(3, 5*b*)311	4.818 072	0.586 156	106.4957
(3, 5*b*)110	4.839 493	0.585 395	106.5164
(3, 5*b*)330	4.863 430	0.584 556	106.5392
(3, 5*d*)311	4.877 417	0.584 072	106.5524
(3, 5*a*)131	4.921 801	0.582 562	106.5934
(3, 5*d*)331	4.948 313	0.581 680	106.6174
(3, 5*c*)121	4.973 987	0.580 839	106.6403
(3, 5*c*)120	5.024 704	0.579 215	106.6845
(3, 5*b*)310	5.040 031	0.578 734	106.6976
(3, 5*c*)130*	5.044 549	0.578 593	106.7014
(3, 5*c*)330*	5.045 078	0.578 577	106.7019
(3, 5*e*)320	5.073 602	0.577 696	106.7259
(3, 5*c*)321	5.078 919	0.577 533	106.7303
(3, 5*e*)131*	5.107 665	0.576 663	106.7540
(3, 5*e*)331*	5.107 934	0.576 655	106.7542
(3, 3*a*)100*	2.355 671	0.860 413	99.0331
(3, 3*a*)311*	2.370 379	0.855 954	99.1544
(3, 3*a*)120*	2.412 464	0.843 644	99.4894
(3, 3*a*)310*	2.454 094	0.832 084	99.8040
(3, 3*a*)111*	2.467 751	0.828 418	99.9037
(3, 3*a*)331*	2.486 609	0.823 456	100.0387
(3, 3*a*)121*	2.502 490	0.819 363	100.1501
(3, 3*a*)320*	2.525 504	0.813 569	100.3077
(3, 3*a*)321*	2.597 784	0.796 363	100.7759
(3, 3*b*)120*	2.604 412	0.794 856	100.8169
(3, 3*b*)100*	2.606 461	0.794 393	100.8295
(3, 3*a*)330*	2.636 122	0.787 805	101.0088
(3, 3*b*)311*	2.643 316	0.786 241	101.0513
(3, 3*a*)131*	2.720 094	0.770 310	101.4848
(3, 3*b*)310*	2.806 190	0.753 978	101.9292
(3, 3*c*)120*	2.857 374	0.744 960	102.1746
(3, 3*b*)111*	2.948 693	0.730 023	102.5810
(3, 4*a*)300*	3.251 126	0.689 218	102.6913
(3, 4*c*)111*	3.270 620	0.686 969	103.7525
(3, 4*b*)320*	3.315 399	0.681 953	103.8890
(3, 3*c*)100*	3.322 360	0.681 191	103.9097
(3, 4*a*)100	3.356 666	0.677 506	104.0100
(3, 4*a*)110*	3.376 221	0.675 456	104.0658
(3, 4*a*)311	3.377 701	0.675 302	104.0700
(3, 4*c*)311*	3.380 754	0.674 986	104.0786
(3, 4*b*)131*	3.401 962	0.672 811	104.1378
(3, 4*b*)321*	3.441 341	0.668 878	104.2448
(3, 4*a*)120	3.445 167	0.668 504	104.2550
(3, 4*d*)120*	3.453 702	0.667 672	104.2776
(3, 4*b*)300*	3.533 074	0.660 223	104.4803
(3, 4*a*)310	3.527 621	0.660 719	104.4668
(3, 4*c*)320*	3.540 072	0.659 590	104.4975
(3, 4*b*)121*	3.540 907	0.659 515	104.4996
(3, 4*a*)331	3.546 557	0.659 007	104.5134
(3, 4*a*)111	3.553 077	0.658 424	104.5292
(3, 4*a*)130*	3.576 699	0.656 338	104.5860
(3, 4*a*)121	3.586 816	0.655 457	104.6100
(3, 4*d*)111*	3.589 605	0.655 216	104.6165
(3, 4*b*)331*	3.607 930	0.653 643	104.6593
(3, 4*a*)320	3.622 332	0.652 424	104.6925
(3, 4*a*)330	3.707 024	0.645 539	104.8798
(3, 4*c*)331*	3.723 344	0.644 266	104.9145
(3, 4*b*)130*	3.728 520	0.643 866	104.9254
(3, 4*d*)320*	3.742 45	0.642 797	104.9545
(3, 4*a*)321	3.743 317	0.642 730	104.9563
(3, 4*b*)120	3.755 444	0.641 810	104.9813
(3, 4*c*)131*	3.759 163	0.641 530	104.9889
(3, 4*b*)110*	3.779 222	0.640 031	105.0297

TABLE III *(continued)*

Classification	Effective quantum number	Energy (a.u.)	Energy (eV)
(3, 4*b*)100	3.786 420	0.639 499	105.0442
(3, 4*b*)311	3.804 180	0.638 200	105.0795
(3, 4*d*)311*	3.812 884	0.637 570	105.0967
(3, 5*d*)131	5.156 034	0.575 231	106.7929
(3, 5*c*)300	5.166 800	0.574 918	106.8014
(3, 5*e*)120	5.182 586	0.574 462	106.8138
(3, 5*b*)111	5.191 949	0.574 194	106.8211
(3, 5*f*)320*	5.195 904	0.574 081	106.8242
(3, 5*f*)120*	5.219 994	0.573 399	106.8428
(3, 6*a*)300	5.229 228	0.573 140	106.8498
(3, 6*c*)111	5.256 422	0.572 385	106.8704
(3, 5*e*)311	5.276 161	0.571 845	106.8851
(3, 6*a*)100	5.308 764	0.570 965	106.9090
(3, 6*b*)320	5.316 965	0.570 746	106.9150
(3, 6*a*)311	5.334 856	0.570 272	106.9278
(3, 5*e*)111	5.378 273	0.569 142	106.9586
(3, 6*a*)110	5.410 067	0.568 332	106.9806
(3, 6*a*)120	5.411 658	0.568 292	106.9817
(3, 6*c*)311	5.414 688	0.568 215	106.9838
(3, 6*b*)131	5.426 483	0.567 919	106.9919
(3, 6*b*)321	5.486 502	0.566 441	107.0321
(3, 6*d*)120	5.501 321	0.566 084	107.0418
(3, 5*c*)100	5.506 077	0.565 970	107.0449
(3, 6*a*)310	5.519 267	0.565 655	107.0535
(3, 6*a*)331	5.519 927	0.565 639	107.0539
(3, 6*a*)111	5.548 564	0.564 963	107.0723
(3, 6*a*)121	5.580 117	0.564 231	107.0922
(3, 6*a*)320	5.604 959	0.563 663	107.1077
(3, 6*b*)300	5.613 390	0.563 472	107.1129
(3, 6*b*)121	5.616 235	0.563 407	107.1146
(3, 6*c*)320	5.627 760	0.563 148	107.1217
(3, 6*a*)130	5.632 986	0.563 031	107.1249
(3, 6*d*)111	5.669 706	0.562 217	107.1470
(3, 6*b*)331	5.670 644	0.562 196	107.1476
(3, 6*a*)330	5.701 229	0.561 531	107.1657
(3, 6*a*)321	5.758 563	0.560 312	107.1989
(3, 6*c*)131	5.759 986	0.560 282	107.1997
(3, 6*c*)331	5.762 761	0.560 224	107.2013
(3, 6*b*)130	5.766 648	0.560 143	107.2035
(3, 6*b*)120	5.775 180	0.559 965	107.2083
(3, 6*b*)100	5.813 842	0.559 170	107.2299
(3, 6*d*)320	5.817 001	0.559 106	107.2317
(3, 6*b*)311	5.823 160	0.558 981	107.2351
(3, 6*b*)110	5.867 736	0.558 088	107.2594
(3, 6*b*)330	5.869 243	0.558 059	107.2602
(3, 6*d*)311	5.907 285	0.557 313	107.2805
(3, 6*a*)131	5.926 307	0.556 946	107.2905
(3, 6*d*)331	5.952 875	0.556 439	107.3043
(3, 6*c*)121	5.985 090	0.555 833	107.3208
(3, 6*c*)120	6.024 590	0.555 103	107.3406
(3, 6*b*)310	6.049 717	0.554 646	107.3530
(3, 6*c*)130	6.049 939	0.554 642	107.3531
(3, 6*c*)330	6.050 642	0.554 629	107.3535
(3, 6*e*)320	6.076 334	0.554 168	107.3660
(3, 6*c*)321	6.087 556	0.553 969	107.3715
(3, 6*e*)331	6.105 965	0.553 644	107.3803
(3, 6*e*)131	6.105 974	0.553 644	107.3803
(3, 6*f*)131*	6.131 236	0.553 203	107.3923
(3, 6*f*)331*	6.131 924	0.553 191	107.3926
(3, 6*d*)131	6.162 879	0.552 658	107.4071
(3, 6*e*)120	6.182 800	0.552 319	107.4164
(3, 6*c*)300	6.190 456	0.552 190	107.4199
(3, 6*f*)320	6.199 789	0.552 033	107.4241
(3, 6*b*)111	6.202 114	0.551 994	107.4252
(3, 7*a*)300	6.226 016	0.551 595	107.4360
(3, 6*f*)120	6.228 992	0.551 546	107.4374
(3, 7*c*)111	6.254 794	0.551 122	107.4489
(3, 6*e*)311	6.274 243	0.550 805	107.4575
(3, 7*a*)100	6.301 519	0.550 366	107.4695
(3, 7*b*)320	6.318 347	0.550 098	107.4768
(3, 7*a*)311	6.328 366	0.549 940	107.4811
(3, 6*e*)111	6.382 732	0.549 093	107.5041
(3, 7*a*)120	6.406 397	0.548 731	107.5140
(3, 7*a*)110	6.417 382	0.548 564	107.5185
(3, 7*c*)311	6.422 225	0.548 491	107.5205
(3, 7*b*)131	6.431 515	0.548 351	107.5243
(3, 7*b*)321	6.494 984	0.547 410	107.5499
(3, 7*d*)120	6.510 189	0.547 189	107.5559
(3, 7*a*)331	6.515 181	0.547 117	107.5579
(3, 7*a*)310	6.518 220	0.547 073	107.5591
(3, 6*c*)100	6.519 465	0.547 055	107.5596
(3, 7*a*)111	6.547 161	0.546 658	107.5704
(3, 7*a*)121	6.579 881	0.546 195	107.5830
(3, 7*a*)320	6.608 728	0.545 792	107.5939
(3, 7*b*)300	6.626 457	0.545 548	107.6006
(3, 7*b*)121	6.627 797	0.545 529	107.6011
(3, 7*c*)320	6.634 505	0.545 437	107.6036
(3, 7*a*)130	6.641 494	0.545 342	107.6062
(3, 7*b*)331	6.679 697	0.544 825	107.6203
(3, 7*d*)111	6.681 882	0.544 795	107.6211
(3, 7*a*)330	6.700 573	0.544 546	107.6279
(3, 7*a*)321	6.758 698	0.543 783	107.6486
(3, 7*c*)131	6.759 274	0.543 775	107.6488
(3, 7*c*)331	6.769 991	0.543 637	107.6526
(3, 7*b*)130	6.773 548	0.543 591	107.6538
(3, 7*b*)120	6.775 890	0.543 561	107.6547
(3, 7*b*)100	6.813 942	0.543 076	107.6679
(3, 7*b*)311	6.822 816	0.542 964	107.6709
(3, 7*d*)320	6.827 594	0.542 904	107.6725
(3, 7*b*)330	6.869 939	0.542 376	107.6869
(3, 7*b*)110	6.879 434	0.542 260	107.6901
(3, 7*d*)311	6.920 339	0.541 761	107.7036
(3, 7*a*)131	6.925 504	0.541 699	107.7053
(3, 7*d*)331	6.954 737	0.541 349	107.7148
(3, 7*c*)121	6.988 408	0.540 952	107.7257
(3, 7*c*)120	7.020 629	0.540 577	107.7359
(3, 7*c*)130	7.050 348	0.540 235	107.7451
(3, 7*c*)330	7.050 574	0.540 233	107.7452
(3, 7*b*)310	7.050 861	0.540 230	107.7453
(3, 7*e*)320	7.076 178	0.539 942	107.7531
(3, 7*c*)321	7.089 240	0.539 795	107.7571
(3, 7*e*)131	7.102 884	0.539 642	107.7613
(3, 7*e*)331	7.103 466	0.539 636	107.7615
(3, 7*f*)131	7.131 714	0.539 323	107.7700
(3, 7*f*)331	7.132 942	0.539 309	107.7704

TABLE IV. Classification of different series for Li^+ below the $N=3$ state of Li^{++}.

Series classification	Lowest n	Approximate mixings	Comments
$^1S^e$, three series involving configurations: $3snp$, $3pnp$, $3dnd$			
$(3,na)\,^1S^e$	3	$(3snp+3pnp)$	
$(3,nb)\,^1S^e$	3	$(3snp-3pnp)-3dnd$	
$(3,nc)\,^1S^e$	3	$(3snp-3pnp)+3dnd$	$(3,3c)$ contains 5% $4f4f$
$^3S^e$, three series involving configurations: $3snp$, $3pnp$, $3dnd$			
$(3,na)\,^3S^e$	4	$(3snp+3pnp)$	
$(3,nb)\,^3S^e$	4	$(3snp-3pnp)-3dnd$	
$(3,nc)\,^3S^e$	4	$(3snp-3pnp)+3dnd$	
$^1P^o$, five series involving configurations: $3snp$, $ns3p$, $3pnd$, $np3d$, $3dnf$			
$(3,na)\,^1P^o$	3	$(3snp+ns3p)+(3pnd+np3d)$	
$(3,nb)\,^1P^o$	3	$(3snp+ns3p)-(3dnf+np3d)$	
$(3,nc)\,^1P^o$	4	$(3snp-ns3p)+(3pnd-np3d)$	
$(3,nd)\,^1P^o$	4	$(3pnd-np3d)+(3snp-ns3p)+3dnf$	
$(3,ne)\,^1P^o$	4	$(3pnd-3dnf)$	10% mixture of other states
$^3P^o$, five series involving configurations: $3snp$, $ns3p$, $3pnd$, $np3d$, $3dnf$			
$(3,na)\,^3P^o$	3	$(3snp+ns3p)+(3pnd+np3d)$	$(3,4a)$ and $(3,4c)$ are mixed because series a and c are crossing in that energy range
$(3,nb)\,^3P^o$	3	$(3snp+ns3p)+3dnf$	
$(3,nc)\,^3P^o$	4	$(3snp-ns3p)+(3pnd-np3d)$	
$(3,nd)\,^3P^o$	4	$(3snp-ns3p)+np3d-3dnf$	
$(3,ne)\,^3P^o$	4	$(3snp-ns3p)-3pnd+3dnf$	
$^1P^e$, two series involving configurations: $3pnp$, $3dnd$			
$(3,na)\,^1P^e$	4	$(3pnp+3dnd)$	both series decay only to $2p$ plus a p-continuum electron
$(3,nb)\,^1P^e$	4	$(3pnp-3dnd)$	
$^3P^e$, two series involving configurations: $3pnp$, $3dnd$			
$(3,na)\,^3P^e$	3	$(3pnp+3dnd)$	both series decay only to $2p$ plus a p-continuum electron. Mixings are not 1:1 (more like 2:1 for a, and 1:2 for b)
$(3,nb)\,^3P^e$	3	$(3pnp-3dnd)$	
$^1D^o$, three series involving configurations: $3pnd$, $np3d$, $3dnf$			
$(3,na)\,^1D^o$	3	$(3pnd+np3d)$	contain 15%df. Series a and b are crossing at $(3,5a)$ and $(3,5b)$
$(3,nb)\,^1D^o$	4	$(3pnd+np3d)$	contain 15% df
$(3,nc)\,^1D^o$	4	$3pnf$	contain 20%pd
$^3D^o$, three series involving configurations: $3pnd$, $np3d$, $3dnf$			
$(3,na)\,^3D^o$	3	$(3pnd+np3d)$	contain 8% $3dnf$
$(3,nb)\,^3D^o$	4	$(3pnd-np3d)$	contain 8% $3dnf$
$(3,nc)\,^3D^o$	4	$3dnf$	contain 20% pd
$^1D^e$, six series involving configurations: $3pnp$, $3snp$, $ns3d$, $3dnd$, $3pnf$, $3dng$			
$(3,na)\,^1D^e$	3	$(3snd+ns3d)-3pnp$	
$(3,nb)\,^1D^e$	3	$(3snd+ns3d)+3dnd$	
$(3,nc)\,^1D^e$	3	$ns3d+3pnp+3pnf-(3dnd-3dng)$	difficult to classify
$(3,nd)\,^1D^e$	4	$(3snd-ns3d)+3pnf$	2:1 sd-to-pf ratio
$(3,ne)\,^1D^e$	4	$3snd+3pnp-3pnf-3dnd-3dng$	difficult to classify
$(3,nf)\,^1D^e$	5	$3dng$	35% other

TABLE IV *(continued)*

Series classification	Lowest n	Approximate mixings	Comments
$^3D^e$, six series involving configurations: $3pnp$, $3snd$, $ns3d$, $3dnd$, $3pnf$, $3dng$			
$(3,na)\,^3D^e$	3	$(3snd+ns3d)$	a and c cross near $n=6$
$(3,nb)\,^3D^e$	4	$(3snd-ns3d)-3pnp$	
$(3,nc)\,^3D^e$	4	$(3snd-ns3d)+3pnf+3dn\,d$	Above $n=5$ crossing causes breakdown of classifications
$(3,nd)\,^3D^e$	4	$3pnp+3pnf-3pnf$	
$(3,ne)\,^3D^e$	4	$(3snd+ns3d)+3pnp-3pnf+3dng$	
$(3,nf)\,^3D^e$	5	$3dng-3pnf$	
$^1F^o$, six series involving configurations: $3snf$, $3pnd$, $np3d$, $3png$, $3dnf$, $3dnh$			
$(3,na)\,^1F^o$	3	$3pnd-np3d+3dnf$	
$(3,nb)\,^1F^o$	4	$3pnd-npsd$	10–15% $3snf$
$(3,nc)\,^1F^o$	4	$3snf+(3png+3dnf-np3d)$	
$(3,nd)\,^1F^o$	4	$3pnd+3png-3dnf$	15% other
$(3,ne)\,^1F^o$	5	$3snf-3png$	25% other
$(3,nf)\,^1F^o$	6	$3dnf$	15% other
$^3F^o$, six series involving configurations: $3snf$, $3pnd$, $np3d$, $3png$, $3dnf$, $3dnh$			
$(3,na)\,^3F^o$	3	$3pnd+np3d$	10% $3snf$
$(3,nb)\,^3F^o$	4	$3snf+np3d$	
$(3,nc)\,^3F^o$	4	$3snf+3dnf$	12% other
$(3,nd)\,^3F^o$	4	$(3pnd-np3d)+(3png-3dnf)$	$(3,4d)$ has 20% $3snf$
$(3,ne)\,^3F^o$	5	$3snf-3png$	20% other
$(3,nf)\,^3F^o$	6	$3dnh$	10% other
$^1F^e$, three series involving configurations: $3pnf$, $3dnd$, $3dng$			
$(3,na)\,^1F^e$	4	$3pnf-3dnd$	
$(3,nb)\,^1F^e$	4	$3pnf+3dnd$	10% $3dng$
$(3,nc)\,^1F^e$	5	$3dng$	15% $3pnf$
$^3F^e$, three series involving configurations: $3pnf$, $3dnd$, $3dng$			
$(3,na)\,^3F^e$	3	$3pnf-3dnd$	
$(3,nb)\,^3F^e$	4	$3pnf+3dnd$	
$(3,nc)\,^3F^e$	5	$3dng$	10% $3pnf$

and 110 eV (c.m. system). The peaks in this spectrum are arbitrarily numbered 1–7. The identifications of these line structures are based on the comparison of the peak energies with the transition energies listed in Tables I, III, and V, respectively. We have assigned the main peaks to transitions of doubly excited Li II states decaying via Coulomb autoionization to the $(1s\epsilon l)^{1,3}l$ continua. This is consistent with the calculations of Balashov *et al.*[30] and Stewart *et al.*[31–33] The experimental autoionization structures are shown in Fig. 8 along with comparisons with the following calculations: (a) the six lowest transition energies of $^1P^o$ resonances deduced from Balashov's calculation[30]; (b) Stewart and co-worker's[31–33] energy values of the configurations $(2s^2)\,^1S$, $(2s2p)^{1,3}P$, and $(2p^2)\,^1S,^1D$ (traditional classification); and (c) the main Li II $^{1,3}S^e$, $^{1,3}P^o$, $^{1,3}D^e$, and $^{1,3}F^o$ energy values above the Li III $1s$ ground state as presented in this paper (see Tables I and III). We have excluded from the figure the $^{1,3}P^e$ and $^{1,3}D^o$ states since they would not produce prompt electrons.

The energy resolution of our apparatus was not sufficient to resolve variations in the cross section of the order of the natural width ($\Gamma < 0.2$ eV), hence the observed Li II autoionization peak heights for transitions to single final states depend only on the excitation cross sections.[13] This is important when relative intensities of lines stemming from different initial levels such as Li II $(2,2a)\,^3P^o$ and Li II $(2,2a)\,^1P^o$, etc., are compared.

From Table I it can be seen that the lowest prompt autoionizing Li II states are $(2,2a)\,^1S^e$, $(2,2a)\,^3P^o$, $(2,2a)\,^1D^e$, and $(2,2a)\,^1P^o$ in order of increasing energy. The theoretical transition en-

TABLE V. Triply excited states in Li, with configurations $^2S^e$ and $^2P^o$.

Classification	No. of Electrons	Energy (a.u.) below total ionization	Energy (eV) above Li ground state	Energy (eV) above 1s threshold	Energy (eV) above $(1s2s)\,^3S$
$1(2s^2 2p)\,^2P^o$	3	2.237 332	142.552	61.567	78.181
$1(2s2p^2)\,^2S^e$	3	2.059 242	147.398	66.413	83.026
2 $^2S^e$	3	2.000 671	148.992	68.007	84.621
$2(2p^3)\,^2P^o$	3	1.992 823	149.206	68.220	84.833
3 $^2P^o$	3	1.977 296	149.628	68.643	85.256
4 $^2P^o$	3	1.957 597	150.164	69.179	85.792
3 $^2S^e$	3	1.946 582	150.464	69.479	86.092
4 $^2S^e$	3	1.935 286	150.771	69.786	86.381
5 $^2P^o$	3	1.930 839	150.892	69.907	86.520
6 $^2P^o$	3	1.924 614	151.062	70.076	86.689
7 $^2P^o$	3	1.906 205	151.562	70.577	87.190
$(2,2a)\,^1S^e$	2	1.902 107	151.674	70.689	87.302
5 $^2S^e$	3	1.876 317	152.376	71.390	88.003
$(2,2a)\,^3P^o$	2	1.874 645	152.421	71.436	88.049
8 $^2P^o$	3	1.863 538	152.723	71.738	88.351
9 $^2P^o$	3	1.856 891	152.904	71.919	88.532
10 $^2P^o$	3	1.853 743	152.990	72.005	88.618
6 $^2S^e$	3	1.835 791	153.478	72.493	89.106
11 $^2P^o$	3	1.821 748	153.861	72.875	89.488
7 $^2S^e$	3	1.801 004	154.425	73.440	90.053
12 $^2P^o$	3	1.800 661	154.434	73.449	90.062
13 $^2P^o$	3	1.798 138	154.503	73.518	90.131
$(2p)^2\,^3P^e$	2	1.790 680 6	154.706	73.721	90.334
Continuum	•••	0	203.4303	122.445	139.058

ergies associated with these states deviate less than 0.5 eV from the centroid of the two strongest peaks (1) and (2), respectively. The strongest peak in the spectrum (1) and about 70 eV can be attributed to decay of the $^1S^e$ and $^3P^o$ states which are predicted at 70.69 and 71.44 eV, respectively. These two levels ($\Delta E = 0.75$ eV) cannot be resolved in our experiments. The positions of the $(2,2a)\,^1D^e$ and $(2,2a)\,^1P^o$ states (Table I) coincide closely with the position of the 2nd strong peak. The correct identification of this peak is also supported by the theoretical estimate of Stewart *et al.* and Balashov *et al.* who predict the transition $(2s2p)\,^1P^o \rightarrow (1s\epsilon p) \times {}^1P^o$ slightly above the experimental line center. The energy separation of the peaks (1) and (2) is 3.3 eV which is very close to the energy separation of 3.46 eV for the $(2,2a)\,^3P^o$ and $(2,2a)\,^1P^o$ levels (see Table I).

We conclude that this measurement gives the first experimental observation of Li II $(2,2a)\,^{1,3}P^o$ states. These results are summarized in Table VII. The uncertainties of our data are purely systematic and include the possible error of the analysis of the spectra due to the underlying $(2,2a)\,^1S^e \rightarrow (1s\epsilon s)\,^1S^e$ and $(2,2a)\,^1D^e \rightarrow (1s\epsilon d)\,^1D^e$ unresolved lines. The observation of the transitions $(2,2a) \times {}^3P^o \rightarrow (1s\epsilon p)\,^3P^o$ and $(2,2a)\,^1P^o \rightarrow (1s\epsilon p)\,^1P^o$ in Li^+

TABLE VI. Decay modes for doubly excited states. States below the $n = 2$ threshold decay only to the 1s continuum. States between the $n = 2$ and $n = 3$ thresholds can decay through all channels listed below.

Initial Configuration	Final decay channels	
$^{1,3}S^e$	$1s\epsilon s$	$2s\epsilon s$
		$2p\epsilon p$
$^{1,3}P^o$	$1s\epsilon p$	$2s\epsilon p$
		$2p\epsilon s$
		$2p\epsilon d$
$^{1,3}P^e$		$2p\epsilon p$
$^{1,3}D^o$		$2p\epsilon d$
$^{1,3}D^e$	$1s\epsilon d$	$2s\epsilon d$
		$2p\epsilon p$
		$2p\epsilon f$
$^{1,3}F^o$	$1s\epsilon f$	$2s\epsilon f$
		$2p\epsilon d$
		$2p\epsilon g$
$^{1,3}F^e$		$2p\epsilon f$

demonstrates that the collective foil excitation populates these states with considerable cross-section. This is of particular interest for measurements on Be (Ref. 34) and B (Ref. 35), since experimental data for doubly excited P states are available only for H^- and He.

For the higher-lying Li II transitions below the $n=2$ series limit a unique interpretation of the experimental features is not possible, in general. However, a small hump just below peak (3) might be associated with the decay of $(2,2B)\,^1S$ at 78.53 eV. Peak (3) cannot be identified on the basis of autoionizing Li II states and will be discussed later. The peak (4) at about 86 eV should not be assigned to a single decay, since many closely spaced transitions (see Table I) are overlapping in this region. Similarly, the peak (5) near 88 eV could be a cumulative effect of many decaying states with effective quantum number $n^* \simeq 4$ (Table I). A multitude of autoionizing levels with effective quantum numbers $n^* \simeq 5$ and $n^* \simeq 6$ (Table I) might be responsible for the shoulder (6) on peak (5).

VII. Li II STATES BETWEEN THE $N=2$ AND $N=3$ SERIES LIMITS

In a nonrelativistic approximation the $N=2$ and $N=3$ levels of Li III are degenerate. As a result of this degeneracy the configuration mixing is strong whenever there are more than one series of equal parity and J values (Tables II and IV). Some exceptions occur for F states. One would expect that these deviations from the independent particle model become even more pronounced when one goes from the $N=2$ to the $N=3$ threshold. For example, for $^1P^o$ states below $N=2$, three series exist (Table II), whereas for $^1P^o$ states between $N=2$ and $N=3$ (Table IV) there are five distinct series, corresponding to heavy configuration interaction of the five configurations: $3snp$, $ns3p$, $3pnd$, $np3d$, $3dnf$.

Figure 9 shows the discrete decay modes of the lowest $^1P^o$ state above $N=2$ specifically $(3,3a)\,^1P^o$. Fano has pointed out that the autoionization channel requiring the least energy transfer is most likely.[23] Thus autoionization of $3\,lnl'(n \geq 3)$ levels leads principally to the $2l\epsilon l'$ continuum. Nevertheless, a small fraction of these Li II states decay to the final ionic state Li III $1s$ (second column of Table VI). In the case of $(3,3a)\,^1P$ (see Fig. 9), the channels leading to the $(2s\epsilon p)\,^1P^o$, $(2p\epsilon s)\,^1P^o$, and $(2p\epsilon d)\,^1P^o$ final states are favored. One expects such low-energy electrons to be ejected by fast moving Li projectiles only in forward directions. The "kinematical cutoff" is defined by[13,36]

$$E_{c.m.} + \epsilon \sin^2\Theta_{lab} = 0\,, \tag{4}$$

where $\epsilon = (m/M)E$ is the reduced projectile energy and Θ_{lab} is the maximum angle of observation (beam axis: $\Theta_{lab}=0°$). For our geometry Θ_{lab} is 42.3°. Substituting this value in the above equation, one can show that all electrons arising from decays of Li projectiles (E: 282 keV) with transition energies less than 10 eV ($E_{lab} < 12$ eV) are outside the range of our spectrometer. Consequently, autoionization of Li II levels below $(3,3a)\,^1F^o$ states (see Table II) decaying into the $2l\epsilon l'$ continuum fall below the kinematic threshold of our electron analyzer. However, those Li II levels positioned above $(3,3a)\,^1F^o$ could contribute to the

TABLE VII. Excitation energies in eV for $(2,2A)\,^{1,3}P^o$ states in Li II (measured from the Li II $1s^2$ ground state).

Experiment $(2,2A)\,^3P$	Theory $(2,2A)\,^3P$	Experiment $(2,2A)\,^1P$	Theory $(2,2A)\,^1P$
146.9±0.5 [a]	147.07 [a]	150.3±0.5 [a]	150.54 [a]
	146.95 [b]		150.31 [b]
			150.59 [c]

[a] This work.
[b] See Chan and Stewart (Ref. 31).
[c] See Balashov *et al.* (Ref. 30).

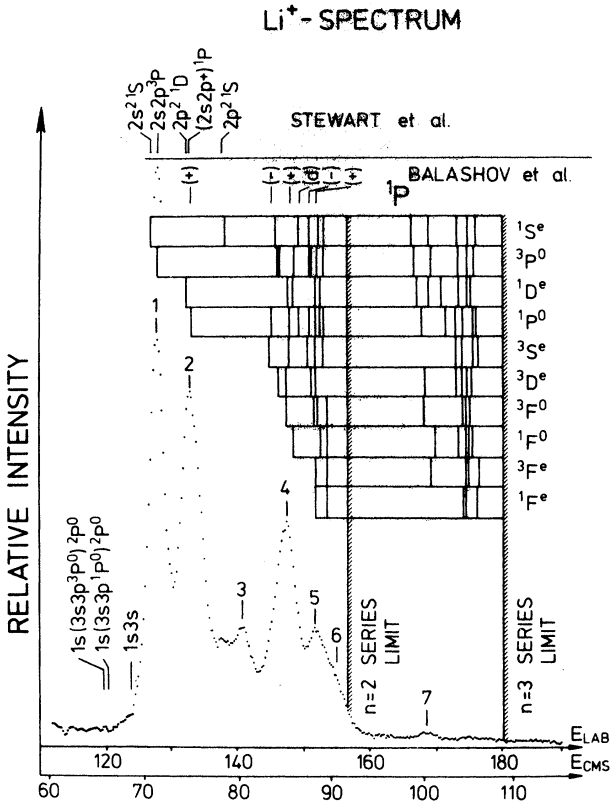

FIG. 8. Li II autoionization spectrum between 60 and 110 eV (background subtracted).

spectrum at low energies. A hump appearing in the prompt spectrum at about $E_{lab}=12$ eV (Fig. 2) might therefore be attributed to such low-energy decays. In addition a small structure (peak 7) above the noise level occurs in the high-energy portion at about 100 eV (Fig. 8) which coincides with several Li II $(3,3a)$, $(3,3b)$, and $(3,3c)$ levels decaying to the $1s\epsilon l$ continuum (Table III). Thus the existence of beam-foil excited Li II levels lying at energies between the second and third ionization limit of Li^{2+} is indicated. An equivalent structure has been seen in the H^- spectrum by Risley and co-workers[13] who identified these narrow peaks as corresponding to autodetachment of $3lnl'$ $(n \geq 3)$ levels.

VIII. TRIPLY EXCITED STATES IN Li I

Recently some work[37,38] has been carried out to investigate the formation and decay of short-lived negative helium ions of the kind $2s^2 2p$, $2s2p^2$, and $2p^3$. For monoenergetic electrons interacting with a helium gas, Fano and Cooper[38] have predicted the formation of the following triply excited He^- resonances: $(2s^2 2p)\,^2P^o$, $(2s2p^2)\,^2S^e$, $^2D^e$, and $(2p^3)\,^2P^o$. Kuyatt, Simpson, and Mielczarek[4] were the first who identified the $(2s^2 2p)\,^2P^o$ and $(2s2p^2)\,^2D^e$ He^- compound states using a transmission experiment. The beam-foil technique has the advantage over elastic electron scattering of being able to produce these states much more abundantly in positive ions. Hence triply excited Li I levels isoelectronic with He^- might contribute to the prompt electron emission after $^7Li^+ \rightarrow$ C-foil collisions. In fact, the high-energy portion of our prompt lithium spectrum (Fig. 8) has revealed an unidentified peak labeled 3 at about 80 eV. We assign this peak as due to Coulomb autoionization of triply excited Li I states for the following reasons: (a) Apparently no transition energies of Li II levels lie between 78.53 and 83.28 eV (see Table I). Therefore peak (3) cannot arise from decays of Li II states. (b) The overlap with Li I transitions as originating from autoionization of the kind $1s3snl$ $(n \geq 3) \rightarrow 1s^2\epsilon l$ must be excluded because these levels are converging at lower energies (68.8 eV) towards the series limit $(1s3s)^3S \infty l \rightarrow 1s^2\epsilon l$ and because these states are decaying predominantly to the final Li II states $(1s2s)^{1,3}S$ and $(1s2p)$ $\times^{1,3}P$, respectively. (c) Finally, this feature at about 80 eV is consistent with energies of triply excited Li I states decaying via Coulomb autoionization to the $(1s2s)^{1,3}S\epsilon l$ and $(1s2p)^{1,3}P\epsilon l$ continua (Table V).

Figure 10 shows the resulting decay scheme for the $(2s^2 2p)\,^2P^o$ and $(2s2p^2)\,^2S^e$ states in Li I where dashed lines are used to represent lower intensity transitions due to shake-down processes. We have compared the experimental lithium spectrum (Fig. 11) around 80 eV with (i) transition energies associated with the levels $(2s^2 2p)\,^2P^o$ and $(2s2p^2)\,^2S$ as derived from Ahmed and Lipsky's TDM calculations[28] (Table V), and (ii) with energy positions of $(2s^2 2p)\,^2P^o$ and $(2s2p^2)\,^2D^e$ decays calculated by the application of a variational method.[39] All transition energies indicated in Fig. 11 are upper limits. We suggest that the structure near 80 eV

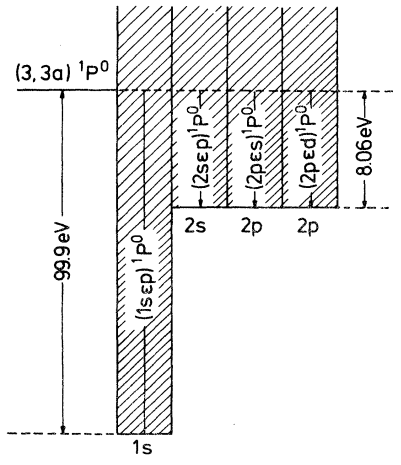

FIG. 9. Decay channels of the Li II $(3,3a)\,^1P^o$ level.

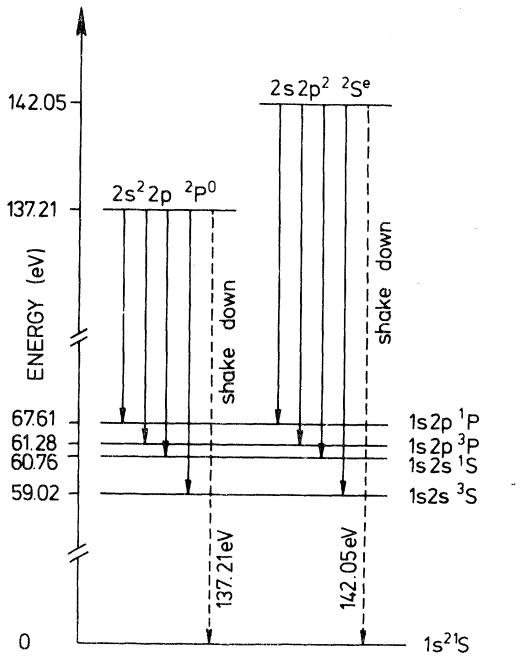

FIG. 10. Schematic drawing of the different competing decay channels of the $(2s^2 2p)\,^2P^o$ and $(2s2p^2)\,^2S^e$ states in Li I (not to scale).

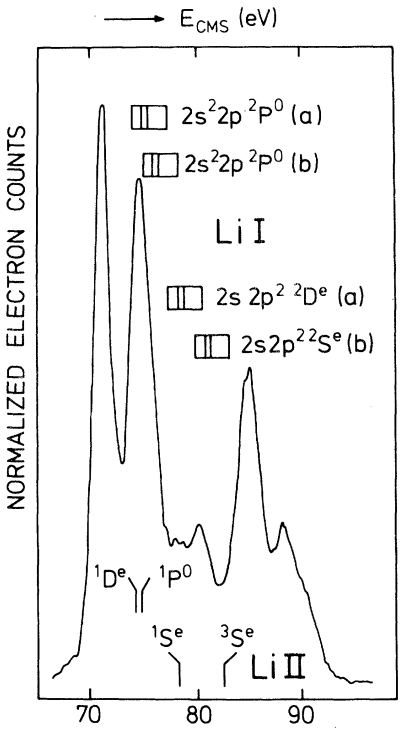

FIG. 11. Comparison of the high-energy portion of the Li spectrum with computed transition energies from autoionizing states of doubly excited Li II and triply excited Li I. (a) Nicolaides (Ref. 39), (b) this paper (Table V) (Ref. 28).

is best assigned to decays of triply excited states. We cannot exclude the possibility that decays of Li I are partially overlapping the decays from Li II levels. For example, the Li II transition $(2, 2a)\,{}^1P^o \rightarrow (1s\epsilon p)\,{}^1P^o$ might coincide with decays of triply excited Li I levels.

IX. CONCLUSION

Using the beam-foil method and observing electrons rather than photons, the decay of short-lived autoionizing states can be studied. We have shown that doubly and triply excited Li I and doubly excited Li II levels are produced with considerable cross sections in $^7Li^+$ – C-foil collisions. This is of particular interest since Li II and Li III levels decaying via dipole transitions might be populated due to cascades of autoionizing states in Li I and Li II.

Because of the insufficient resolution at about 300 keV beam energy a unique interpretation of the observed line structures is difficult except for the most prominent peaks. However, by using thinner foils or gas targets and higher beam energies it is expected that the resolution can be improved. Furthermore, by measuring electrons in coincidence with ions it is hoped that the charge state coordination of the lithium spectra might be obtained.

ACKNOWLEDGMENTS

The authors are indebted to Professor E. Matthias for suggesting the study of electron spectra from foil-excited beams. We should like to thank Professor J. H. Macek for discussing the results with us. We are especially grateful to W. Wittman for his capable assistance in the experimental work. We thank the Deutsche Forschungsgemeinschaft for financial support. The computational work for this paper was carried out at the University of Nebraska's Computing Facility.

[1] J. W. Cooper, U. Fano, and F. Prats, Phys. Rev. Lett. 10, 518 (1963).
[2] I. A. Sellin, Nucl. Instrum. Methods 110, 477 (1973), and references quoted therein.
[3] J. A. Simpson, S. R. Mielczarek, and J. W. Cooper, J. Opt. Soc. Am. 54, 269 (1964).
[4] C. E. Kuyatt, J. A. Simpson, and S. R. Mielczarek, Phys. Rev. 138, A385 (1965).
[5] D. L. Ederer, T. Lucatorto, and R. P. Madden, Phys. Rev. Lett. 25, 1537 (1970).
[6] W. Mehlhorn, Phys. Lett. 21, 155 (1966).
[7] M. E. Rudd and J. H. Macek, Case Studies At. Phys. 3, 47 (1972).
[8] P. Ziem, thesis (1974) (unpublished).
[9] I. Martinson and A. Gaupp, Phys. Rep. 15C, (1974).
[10] I. Martinson, Phys. Scr. 9, 281 (1974).
[11] K. D. Sevier, *Low Energy Electron Spectrometry* (Wiley-Interscience, 1972).
[12] E. B. Bas, U. Banninger, and P. Keller, J. Vac. Sci. Technol. 2, 306 (1972).
[13] J. S. Risley, A. K. Edwards, and R. Geballe, Phys. Rev. A 9, 1115 (1974).
[14] H. G. Berry, J. Desesquelles, and M. Dufay, Nucl. Instrum. Methods 110, 43 (1973).
[15] J. P. Buchet, A. Denis, J. Desesquelles, and M. Dufay, Phys. Lett. 28A, 529 (1969).
[16] M. Levitt, R. Novick, and P. D. Feldman, Phys. Rev. A 8, 130 (1971).
[17] S. T. Manson, Phys. Rev. A 3, 147 (1971).
[18] E. Holøien and S. Geltman, Phys. Rev. 153, 81 (1967).
[19] J. D. Garcia and J. E. Mack, Phys. Rev. 138, A987 (1965).

[20]P. Feldman and R. Novick, Phys. Rev. 160, 143 (1967).
[21]J. P. Buchet, M. C. Buchet-Poulizac, H. G. Berry, and G. W. F. Drake, Phys. Rev. A 7, 922 (1973).
[22]J. W. Cooper, M. J. Conneely, K. Smith, and S. Ormonde, Phys. Rev. Lett. 25, 1540 (1970).
[23]U. Fano and J. W. Cooper, Phys. Rev. 137, A1364 (1965).
[24]B. Fricke (private communication).
[25]L. Lipsky and A. Russek, Phys. Rev. 142, 59 (1966).
[26]P. L. Altick and E. N. Moore, Phys. Rev. Lett. 15, 100 (1965).
[27]L. Lipsky, M. J. Conneely, and R. Anania (unpublished); L. Lipsky, M. J. Conneely, and S. Ormonde, in *Proceedings of the Sixth International Conference on the Physics of Electronic and Atomic Collisions* (MIT, Cambridge, Mass., 1969), p. 1026.
[28]M. Ahmed and L. Lipsky, Phys. Rev. A 12, 1176 (1975); M. Ahmed, Ph.D. thesis (University of Nebraska, 1974) (unpublished).
[29]L. Lipsky, M. Ahmed, and M. J. Conneely, in *Proceedings of the Seventh International Conference on the Physics of Electronic and Atomic Collisions* (North-Holland, Amsterdam, 1971), Vol. 2, p. 917.
[30]V. V. Balashov, S. J. Grishanova, H. M. Kruglowa, and V. Senashenko, Opt. Spectrosc. 28, 466 (1970).
[31]Y. M. C. Chan and A. L. Stewart, Proc. Phys. Soc. Lond. 90, 619 (1967).
[32]R. H. Perrott and A. L. Stewart, J. Phys. B 1, 381 (1968).
[33]R. H. Perrott and A. L. Stewart, J. Phys. B 1, 1226 (1968).
[34]R. Bruch, G. Paul, J. Andrä, and B. Fricke (unpublished).
[35]R. Bruch, G. Paul, and J. Andrä (unpublished).
[36]D. J. Pegg, I. A. Sellin, R. Peterson, J. R. Mowat, W. W. Smith, M. D. Brown, and J. R. MacDonald, Phys. Rev. A 8, 1350 (1973).
[37]G. J. Schulz, Rev. Mod. Phys. 45, 378 (1973).
[38]U. Fano and J. W. Cooper, Phys. Rev. 138, A400 (1965).
[39]C. Nicolaides, Nucl. Instrum. Methods 110, 231 (1973).